*Article*

# Quantification of Alpine Metamorphism in the Edolo Diabase, Central Southern Alps

**Marco Filippi** [1,2] [iD]**, Davide Zanoni** [1] [iD]**, Gisella Rebay** [3] [iD]**, Manuel Roda** [1,*] [iD]**, Alessandro Regorda** [1] [iD]**, Jean-Marc Lardeaux** [2,4] [iD] **and Maria Iole Spalla** [1] [iD]

1 Dipartimento di Scienze della Terra "A. Desio", Università degli Studi di Milano, 20133 Milano, Italy
2 UMR Géoazur, Observatoire de la Côte d'Azur, CNRS, IRD, Université Côte d'Azur, 06560 Valbonne, France
3 Dipartimento Di Scienze Della Terra e Dell'Ambiente, Università degli Studi di Pavia, 27100 Pavia, Italy
4 Center for Lithospheric Research, Czech Geological Survey, 11821 Praha, Czech Republic
* Correspondence: manuel.roda@unimi.it

**Abstract:** The Southern Alps are the retro-vergent belt of the European Alps that developed from Late Cretaceous subduction to Neogene times. The most prominent Alpine thrusts and folds, nowadays sealed off by the Adamello intrusion, were already developed before the continental collision and clasts derived from the eroded pre-collisional wedge can be found in the Cretaceous foredeep sequences. In contrast, the thermal state attained by the Southern Alps during the long-lasting Alpine evolution is still unknown. This contribution provides evidence for Alpine metamorphism in the northern part of the central Southern Alps. Metamorphic conditions are determined for the alkaline Edolo diabase dykes that emplaced in the exhumed Variscan basement rocks before being deformed during the Alpine convergence (D3). The Alpine foliation in the Edolo diabase dykes is marked by actinolite, biotite, chlorite, epidote, albite, and titanite and it developed under greenschist facies conditions at temperature of 350–420 °C and pressure ≤0.2 GPa. The T/depth ratio indicates a minimum of 50–60 °C/km that is compatible with thermal gradients characteristic of arc settings. Based on radiometric ages from the literature, these conditions were attained during the Alpine subduction.

**Keywords:** upper plate metamorphism; Alpine subduction; alkaline magmatism

## 1. Introduction

Crustal thickening due to continental collision is well documented in the external domains of the Alps since the late Eocene (e.g., [1–3] and refs. therein). At that time, flysch deposits and molasses filled the Alpine foreland basins (e.g., [4] and refs. therein) and collisional structures developed in the Helvetic domain under greenschist facies conditions (e.g., [5–9]). Differently, crustal thickening in the Alpine retro-belt (the Southern Alps) started as early as the Late Cretaceous during oceanic subduction and lasted up to post-collisional stages in Eocene to Neogene times [10,11].

Alpine metamorphic minerals are already recognized in the central Southern Alps, but a tectonic interpretation of the Alpine metamorphism is lacking [12–21]. In this contribution, we quantify the Alpine metamorphism in the northern part of the central Southalpine basement, focusing on the alkaline Edolo diabase dykes [22] and combining high-resolution structural analysis with mineral chemistry and P-T estimates. The P-T conditions estimated for the metamorphism in the Edolo diabase dykes are here used to depict the thermal state affecting the Alpine retro-belt during the Alpine convergence.

## 2. Geological Setting

The Alpine convergence involved the subduction of the Alpine Tethys Ocean underneath the Adria plate and the subsequent continental collision with the European lithosphere in Cretaceous to Oligocene times [1–3]. The Southalpine domain is that portion

of Adria plate that was affected by thrusting and folding at shallow crustal levels in the Alpine retro-belt [23].

The Southalpine domain west of the icarie fault consists of Variscan basement rocks and early Permian to Cretaceous sedimentary sequences (Figure 1; [16,19,24,25] and refs. therein). To the north, this domain is separated from the other tectonic units of the Alps by the Periadriatic fault system (Figure 1), a regional scale dominantly strike-slip system that has been active at least since the Oligocene, concurrently with the Bregaglia and Adamello calc-alkaline intrusions [26–29]. This tectonic lineament separates continental and oceanic units belonging to the axial part of the chain that during the Alpine convergence experienced intense deformation and metamorphism (the Austroalpine and Penninic domains) from rocks belonging to the upper plate (the Southalpine domain) that recorded deformation at shallow structural levels (e.g., [30–33]).

The basement of the central Southern Alps consists of different tectono-metamorphic units (TMUs) that heterogeneously record the Variscan evolution and, in the Como Lake area, also the high thermal signature of the Triassic rifting [16,34–36]. The dominant fabric in the Variscan basement in the Adamello area is the late-Variscan S2 foliation, which developed under greenschist facies conditions during coupling of Variscan basement rocks retaining contrasting tectono-metamorphic evolutions (TMUs; [25,36,37] and refs. therein). A minimum age for S2 is constrained by the deposition of Permian siliciclastic sequences, which contain clasts deriving from the Variscan TMUs [19,24,25,38–43]. Variscan Pre-D2 foliations are marked by epidote-amphibolite and/or amphibolite facies minerals ([24,25,37] and refs. therein).

The main Alpine feature of the central Southern Alps is the south-verging Orobic–Porcile–Gallinera thrust system (Figure 1) that has brought Variscan basement rocks onto Permian to Mesozoic covers (e.g., [15,18,20,44–48]). In the footwall, anticlines involving basement and Permian–Mesozoic sequences - i.e. Orobic, Trabuchello–Cabianca, and Cedegolo anticlines (Figure 1) - are interpreted as fault-bend folds formed during on-going southward thrusting in pre-Oligocene times [11,13,14]. In the hanging wall, the most prominent Alpine structures are steeply dipping chevron folds in the Variscan basement (e.g., [16,21,47]). The Adamello calc-alkaline batholith, dated at 43–33 Ma ([49] and refs. therein), crosscuts the Orobic–Porcile–Gallinera thrust system and Cedegolo anticline (Figure 1; [13,14]). A further reactivation of the Periadriatic fault system and Orobic–Porcile–Gallinera thrust system, mostly as dextral strike-slip or transpressional faults, has been envisaged since the late Eocene ([11] and refs. therein).

The age of the syn-subductive activity of the Orobic–Porcile thrust system is constrained by $^{40}$Ar/$^{39}$Ar dating of pseudo-tachylytes at 80–43 Ma ([10] and refs. therein), whereas Cenomanian–Campanian flysches in the southernmost part of the central Southern Alps testify the erosion of both basement and cover units on an active margin propagating southwards [50]. Poorly investigated greenschist facies mylonites are supposed to have accommodated first increments of crustal shortening before the Oligocene (e.g., [17,20,47]). Barometric estimates on pseudotachylites along the Southern Grigna Fault (Figure 1) indicate that this portion of central Southern Alps was buried up to depth equivalent to 0.1–0.2 GPa during the Alpine convergence [51].

Calc-alkaline mafic dykes are widespread in the central Southern Alps (Figure 1), where they crosscut regional scale thrusts and folds in the Variscan basement and Permian to Mesozoic sedimentary sequences [52,53]. The age of these intrusives ranges between 42 and 34 Ma [52,53], confirming that most of the central Southern Alps architecture already existed before the Oligocene [10,11,13,14].

Other mafic dykes, historically known as "Edolo diabases" [22,53], occur between the Periadriatic fault system and Gallinera Thrust (Figure 1). These dykes are characterized by alkaline affinity and are crosscut by the Adamello tonalite. For these reasons a Triassic emplacement is supposed by Italian authors of the past century [22]. Magmatic minerals are dark brown amphibole and biotite, pink clinopyroxene, plagioclase, ilmenite, magnetite,

and rare quartz. Mineral assemblages and whole rock composition [22,53] allow classifying the Edolo diabases as camptonites, a type of alkaline lamprophyres [54,55].
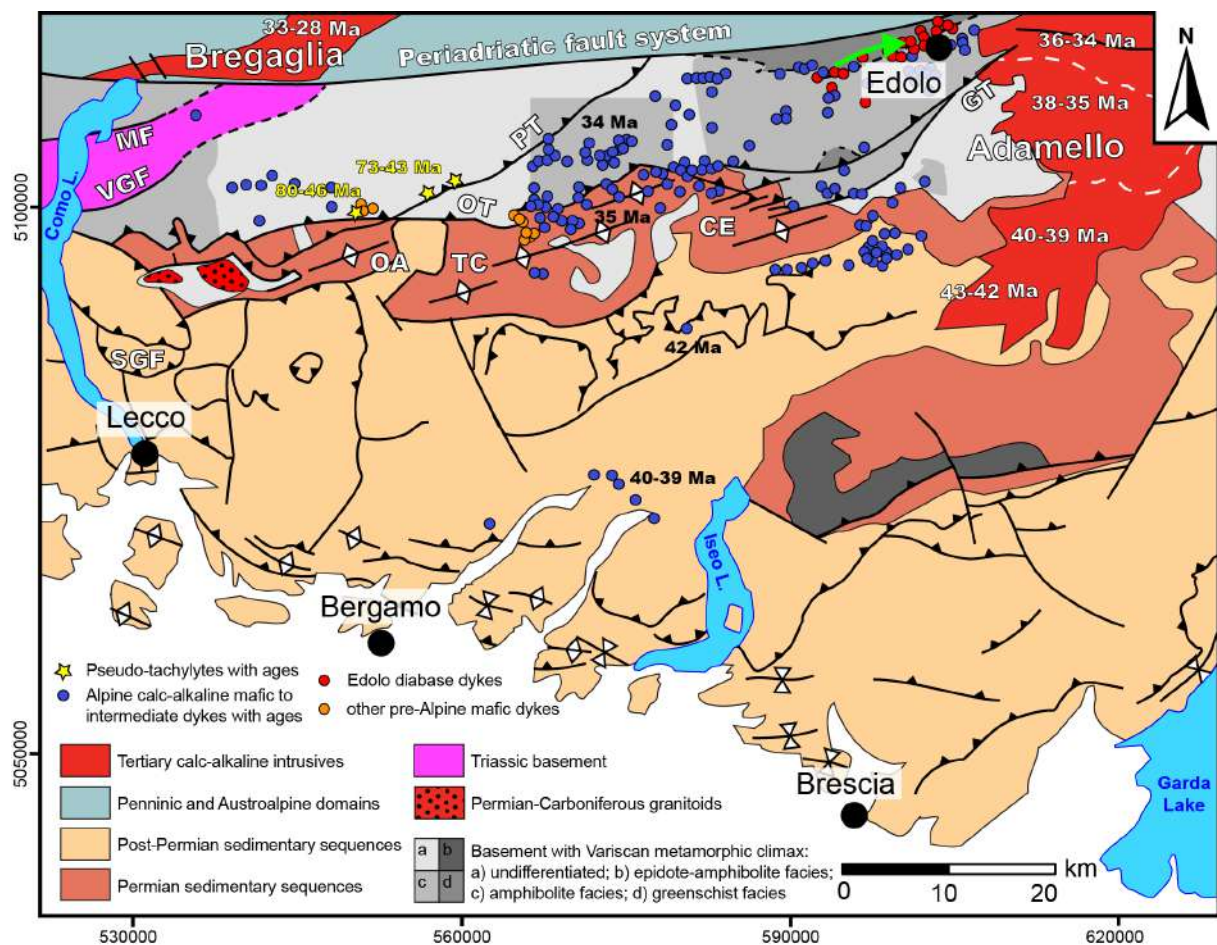


**Figure 1.** Tectonic outline of the central Southern Alps (modified after [11,24,36] and refs. therein). Projected coordinate system: WGS84-UTM32N. Abbreviations–CE: Cedegolo anticline; GL: Gallinera thrust; MF: Musso fault; OA: Orobic anticline; OT: Orobic thrust; PT: Porcile thrust; SGF: Southern Grigna fault; TC: Trabuchello–Cabianca anticline; VGT: Val Grande fault. Adamello ages are from [49]; Bregaglia ages are from [28]; Alpine pseudo-tachylyte ages are from [10]; Tertiary calc-alkaline dyke ages are from [53]. The light green arrow points the studied area.

## 3. Field Occurrence

The studied rocks are located between the Gallinera Thrust and the Periadriatic fault system in the northern part of the central Southern Alps (Figure 1). This area comprises Variscan basement rocks including metapelites, quartzites, minor metabasites, and marbles, in which the dominant fabric is the S2 Variscan foliation marked by low greenschist facies minerals. Upper greenschist to epidote amphibolite facies minerals are relics in low strain domains [19,21]. South of the Gallinera Thrust, S2 is truncated by Permian cover sequences (e.g., [19,25]).

The Alpine deformation (D3) in the Variscan basement results in localized chevron folds of metric wavelength (Figure 2), locally associated with differentiated axial plane foliation (S3). D3 structures are intersected by the Adamello towards the east and by calc-alkaline mafic dykes in different localities [13,14,16,17,19,21,47,53,56]. Biotite- and amphibole-bearing S3 Alpine foliation has been already described in pre-Alpine mafic dykes at the junction between the Porcile and Orobic thrusts [20]. D3 structures are interpreted as syn-kinematic with the Orobic–Porcile–Gallinera thrust system [16,17,21,47] whose age is constrained between 80 and 43 Ma ([10] and refs. therein).

The Edolo diabase occurs in up to 50 m-thick dykes that are mostly characterized by medium grained phaneritic texture (Figure 2), whereas the thinnest dykes are por-phyritic [21,22]. The intrusive contacts with country rocks are characterized by fine grain size. Locally, the dykes host albite-rich late-intrusive veins. The Edolo diabase dykes truncate S2 in the host Variscan basement rocks and are weakly folded (D3) and intersected by the Alpine foliation S3 (Figure 2).



**Figure 2.** Mesotructural characters of foliated Edolo diabase dykes and Variscan country rocks. (**A**): a meter-thick dyke intruded into Variscan basement rocks near Edolo; (**B**,**C**): detail of Alpine S3 foliation developed within a dyke. (**D**): D3 chevron-type Alpine folds in Variscan metapelites; (**E**): a dyke intersecting S2. S2 is affected by Alpine folding (D3), S3 is developed in the dyke. The dyke wall (DW) is at low angle with S3.

## 4. High Resolution Mapping

Structural mapping has been performed at 1:1000 scale along the road-cut between Nembra and Vico villages, less than 2 km west of Edolo (Figure 3). Here, the Edolo diabase dykes are hosted in micaschists, quartz-schist, and quartzite. NNW-dipping S2 is the dominant fabric of the host rocks and is marked by chlorite, white mica, and quartz ribbons; in low-strained domains, the older Variscan foliation (S1) is preserved along D2 isoclinal fold limbs. Alpine D3 folds are chevron-type and metric in wavelength, with sub-horizontal NE-SW trending axes (A3), axial planes (PA3) steeply dipping towards NW or SE (Figure 3), locally associated with an axial plane foliation (S3). The orientation of D2 and D3 structures in the studied area is compatible with that of D2 and D3 structures north of the Orobic–Porcile–Gallinera thrust system (Figure 3; [16,18,20,21,47,48,57]). Geometric compatibility and coherent overprinting relationships between D2 and D3 allow us to interpret D3 structures as Alpine in age, in agreement with the detailed structural analysis performed at regional scale. (e.g., [19,21] and refs therein).

Meter-thick E-W striking Edolo diabase dyke walls are steeply dipping and truncate S2 (Figure 3). Although the limited exposure precludes continuous dyke wall mapping along strike, the detailed structural analysis reveal that the dykes are gently folded during D3, in contrast to the prominent D3 folds recorded in the country rocks. Despite of gentle folding, S3 is locally developed within the Edolo diabase dykes (Figure 3). Within the dykes, S3 strike deviates at least 20° from that of the dyke walls and matches the orientation of PA3 and S3 in the host rocks (Figure 3). Kink-bands, cataclastic shear zones, and minor faults intersect all the structures and lithotypes (Figure 3).
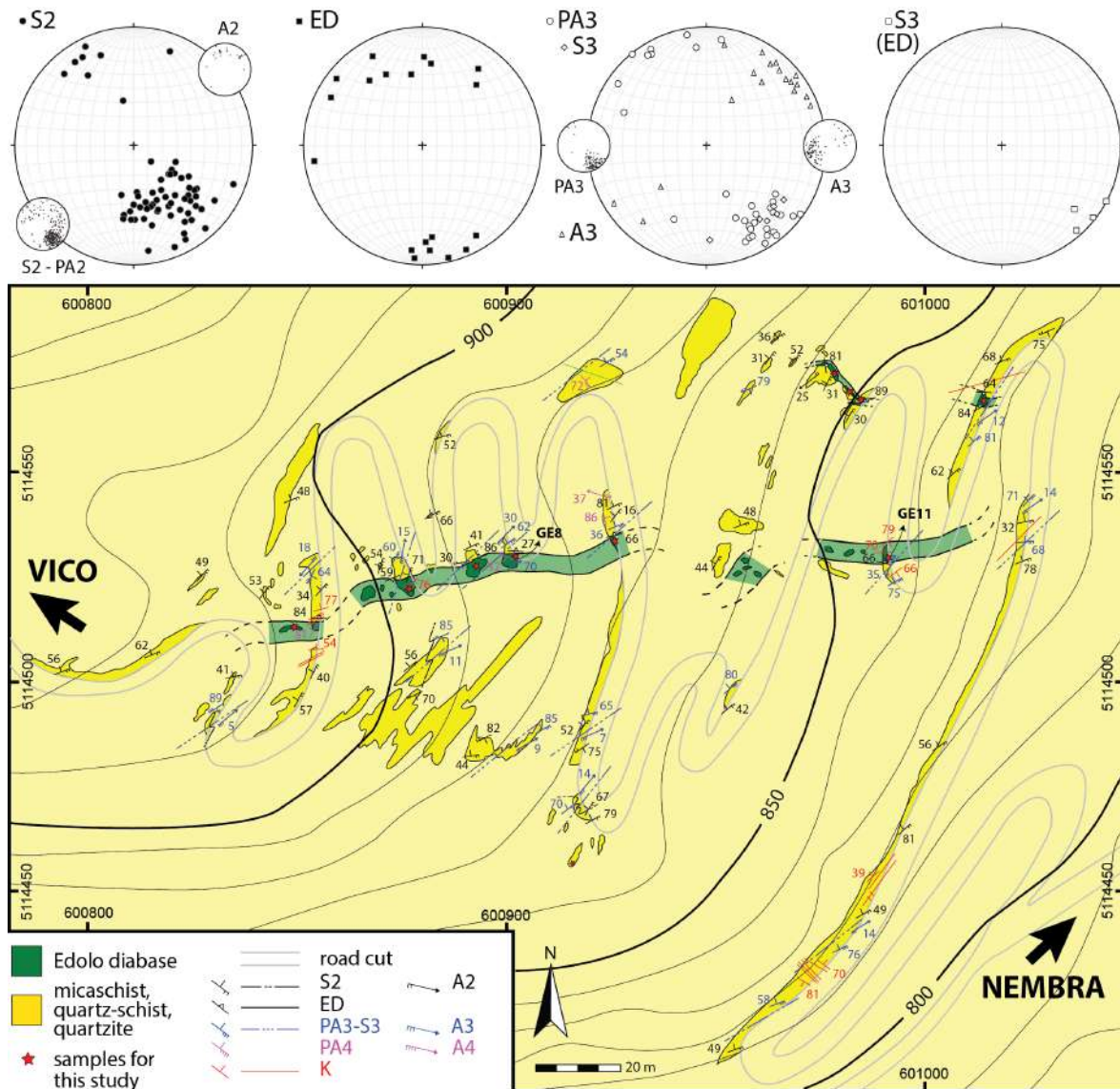


**Figure 3.** Structural map along the road cut from Nembra to Vico villages. Red stars locate samples. Projected coordinate system: WGS84-UTM32N. Stereonets (Schmidt equal-area, lower hemisphere) are referred to different structures and rock types (ED: Edolo diabase). Smaller projections represent structural data included for comparison [21]. Light colours indicate intepreted rock distribution below cover. Red stars locate samples for this study. Mineral chemical analyses are provided for samples Ge8 and Ge11.

## 5. Microstructure

Edolo diabase dykes are composed of euhedral to subhedral crystals of magmatic (I) clinopyroxene (CpxI), amphibole (AmpI), brown biotite (BtI), plagioclase (PlI), ilmenite (IlmI), and apatite (Figure 4). The dyke margins are often porphyritic with millimeter-

sized phenocrysts of AmpI, CpxI, and BtI in an aphanitic groundmass. Cores of magmatic amphiboles are dark brown (AmpI$_1$), locally with pale brown rims (AmpI$_2$). CpxI is pale pink, core to rim zoned (CpxI$_1$ to CpxI$_2$) and locally rimmed by BtI, AmpI$_1$, or AmpI$_2$. Rare ilmenite grains (IlmI) are included in CpxI, AmpI, and BtI. Magmatic plagioclase (PlI) is zoned, with simple to polysynthetic growth-twinning at cores and no twinning at rims. In the phaneritic dykes, interstitial domains between laths of PlI are filled by BtI, AmpI$_2$, rare quartz grains, and magmatic epidote (EpI, Figure 4). At rims, EpI is partially replaced by fine-grained aggregates of metamorphic epidote.
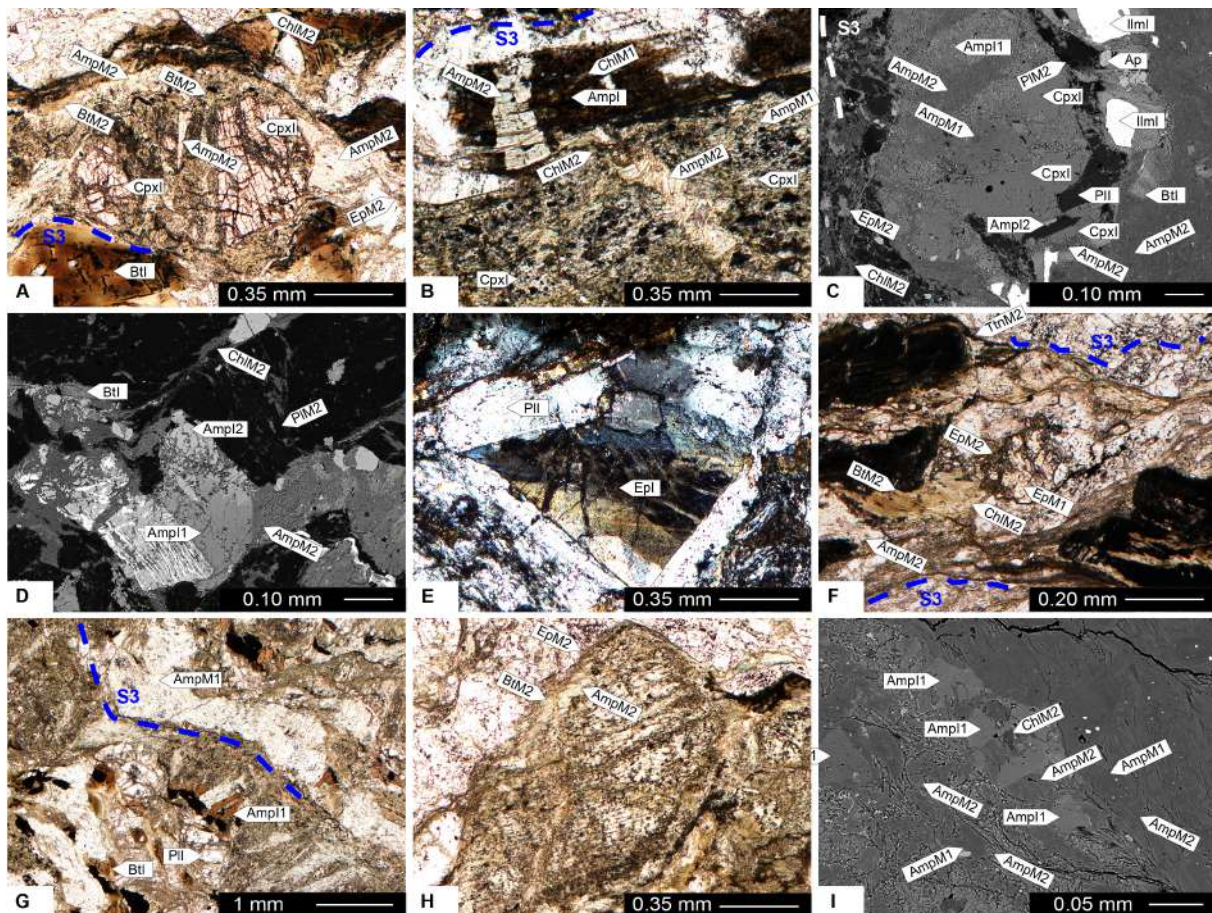


**Figure 4.** Microstructures of Edolo diabase dykes (plane-polarized light and back-scattered electron images). (**A**): CpxI and BtI wrapped by S3. S3 is marked by AmpM$_2$, BtM$_2$, ChlM$_2$, and trails of EpM$_2$ and TtnM$_2$. BtI is parallelized to S3. AmpM$_2$ fills syn-kinematic fractures and pressure shadows around CpxI; (**B**): CpxI and AmpI are pervasively replaced by ChlM$_1$, AmpM$_1$, and titanite. Fractures in AmpI and CpxI are syn-kinematic with S3 and filled by AmpM$_2$ and ChlM$_2$; (**C**): AmpI, BtI, IlmI, PlI, and CpxI (rimmed by Amp I$_2$) are wrapped by S3 that is marked by AmpM$_2$, ChlM$_2$, and EpM$_2$. Boudin necks are filled by AmpM$_2$, PlI is rimmed by PlM$_2$; (**D**): S3 marked by AmpM$_2$, ChlM$_2$, and PlM$_2$. AmpM$_2$ fills pressure shadows around zoned AmpI; (**E**): Interstitial EpI between PlI laths; (**F**): Relics of EpM$_1$ within S3 marked by AmpM$_2$, BtM$_2$, ChlM$_2$, EpM$_2$, and stylolitic films of TtnM$_2$; (**G**): Relics of magmatic minerals and AmpM$_1$-rich layers within inflected S3; (**H**): Relic of CpxI wrapped by S3 supported by AmpM$_2$, BtM$_2$, EpM$_2$ and minor ChlM$_2$; (**I**): Micro-boudins of AmpI aligned in S3 foliation: boudin necks are filled by AmpM$_2$ and ChlM$_2$. In the AmpM$_1$-rich layer to the right, dark gray cores of AmpM$_1$ (Al- and Fe-poor) are rimmed by light gray AmpM$_2$ (Al- and Fe-rich), which marks S3.

Magmatic minerals are locally replaced by post-magmatic mineral assemblages, namely M$_1$ and M$_2$. M$_1$ minerals display coronitic texture and pre-date the Alpine foliation S3. AmpI, BtI, and CpxI are rimmed by coronitic pale green/colorless amphibole (AmpM$_1$),

chlorite ($ChlM_1$), titanite ($TtnM_1$), epidote ($EpM_1$), pyrite, and rare calcite (Figure 4). $M_1$ minerals are interpreted as related to late- to post-magmatic hydrothermal circulation, which affected the dykes soon after their emplacement.

The Alpine S3 foliation in the Edolo diabase dykes is pervasive in centimeter-thick cleavage bands and is marked by $M_2$ minerals (Figure 4), including amphibole ($AmpM_2$), biotite ($BtM_2$), chlorite ($ChlM_2$), epidote ($EpM_2$), plagioclase ($PlM_2$), and titanite ($TtnM_2$)-rich stylolitic films. $M_2$ minerals fill D3 syn-kinematic boudin necks and pressure-shadows around magmatic and $M_1$ minerals (Figure 4). $M_2$ minerals also support micro-shear surfaces at a low angle with S3. In the high strained domains magmatic plagioclase grains are fractured. Pre-Alpine $AmpM_1$-rich veins are transposed along S3 (Figure 4). $M_2$ minerals form coronae around magmatic and $M_1$ hydrothermal minerals in the low-strained domains.

In quartzites, the dominant S2 foliation is marked by preferred orientation of medium- to coarse-grained quartz lithons and films rich in opaque minerals and rare white mica. In quartz-schists, white mica and elongated opaque mineral films mark the dominant foliation S2. Often these rocks record D3 Alpine thight folds with quartz layers thickened in the hinge zone. In micaschists, the pervasive S2 foliation is marked by white mica and chlorite. Rare tourmaline shows sharp grain boundaries against white mica marking S2. Only locally, quite fresh biotite is particularly abundant in the films of S2 along with relict biotite crystals between films. Quartz occurs in micro-lithon domains. White mica and biotite prophyroclasts are wrapped by S2, the latter partially replaced by chlorite and white mica and quartz filling the strain-shadows. Relict porphyroclasts are completely replaced by white mica and chlorite. Folded S1 foliation is marked by quartz layers and white mica films. S2 foliation is crenulated by D3 Alpine folds and the rare crenulation cleavage S3 is marked by white mica and chlorite.

## 6. Mineral Chemistry

Two foliated (S3) samples of Edolo diabase (Ge8, Ge11; Figure 3) were analyzed at Università degli Studi di Milano with a JEOL 8200 Super Probe (WDS) at 15 kV accelerating voltage and with a beam current of 5 nA; natural silicates served as standards. Amphibole formulae are calculated using Locock's amphibole classification spreadsheet [58] and following IMA 2012 recommendations. Clinopyroxene formula is recalculated at 4 cations and 6 O, feldspar at 4 O, epidote at 8 cations and 12.5 O. Biotite and chlorite are recalculated at 11 and 7 O, respectively. Representative mineral analyses are in Table S1.

### 6.1. Magmatic Minerals

$CpxI_1$ ($X_{Mg}$ = 0.69–0.78) and $CpxI_2$ ($X_{Mg}$ = 0.63–0.68) are diopside, with $CpxI_1$ slightly Al- and Ti- richer (Al = 0.14–0.30 apfu, Ti = 0.04–0.08 apfu) than $CpxI_2$ (Al = 0.05–0.18, Ti = 0.00–0.04 apfu).

$AmpI_1$ (Figure 5) is ferri-kaersutite, Ti-rich ferro-pargasite, or Ti-rich magnesio-hornblende, with Si = 5.99–6.34 apfu, Ti = 0.45–0.64 apfu, and Al = 1.90–2.32 apfu. $AmpI_1$ is characterized by Na varying from 0.40 to 0.86 apfu and K from 0.18 to 0.25 apfu, as reflective of the alkaline affinity of the Edolo diabase dykes (cfr. [59]). $AmpI_1$ $X_{Mg}$ in sample Ge8 (0.45–0.49) is slightly lower than in sample Ge11 (0.49–0.66).

$AmpI_2$ (Figure 5) is (Ti-rich) ferro-pargasite similar to $AmpI_1$ in terms of Si, Al, Na, and K contents, but markedly Ti poorer (Ti = 0.14–0.44 apfu) and Fe richer ($X_{Mg}$ = 0.16–0.33), with the lowest $X_{Mg}$ values in sample Ge8. BtI is characterized by $Al^{VI}$ from 0.00 to 0.38 apfu and Ti from 0.37 to 0.78 apfu. BtI $X_{Mg}$ in sample Ge8 (0.43–0.44) is lower than in sample Ge11 (0.44–0.49).

Zoned PlI is $An_{40-58}$ at core, $An_{10-38}$ between core and rim, and $An_{7-8}$ at rim. EpI filling interstices between PlII is characterized by $Fe^{3+}$ = 0.36–0.53 apfu and $Al^{VI}$ = 2.47–2.64 apfu; EpI rimming BtI is $Fe^{3+}$ richer (0.54–0.59 apfu) and $Al^{VI}$ poorer (2.41–2.46 apfu).
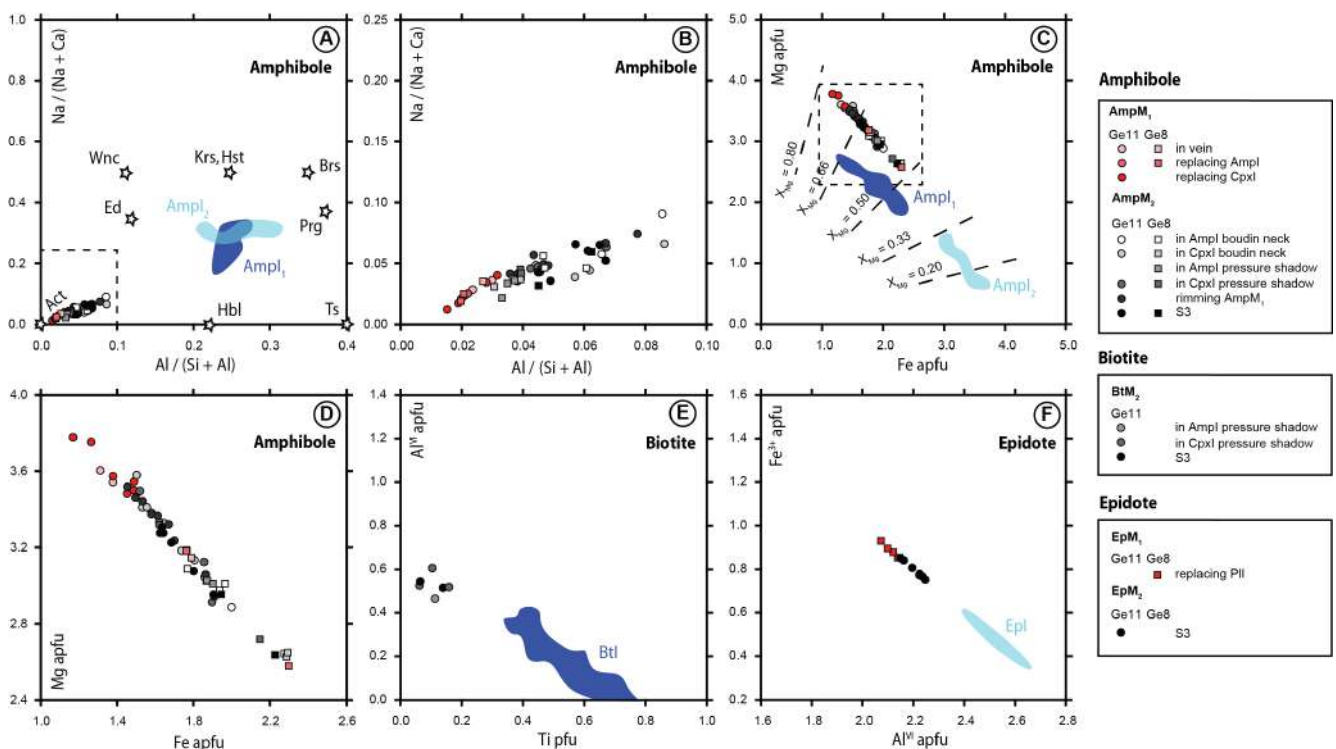
**Figure 5.** Composition of magmatic ($I_1$, $I_2$) and metamorphic ($M_1$, $M_2$) minerals in the Edolo diabase. Compositional variations in $I_1$ and $I_2$ minerals are reported as blue and light blue shaded areas, respectively. Compositions of $M_1$ and $M_2$ minerals are plotted as circles (sample Ge11) and squares (sample Ge8). Red shades highlight different microstructural sites occupied by hydrothermal $M_1$ minerals. Black shades highlight different microstructural sites occupied by Alpine $M_2$ minerals. (**A**): Al/(Al + Si) vs. Na/(Na + Ca) amphibole diagram. Compositional end-members are reported as stars; (**B**): Enlargement of A. (**C**): Fe vs. Mg amphibole diagram. $X_{Mg}$ isolines are reported as dashed lines; (**D**): Enlargement of C; (**E**): Ti vs. $Al^{VI}$ biotite diagram; (**F**): $Al^{VI}$ vs. $Fe^{3+}$ epidote diagram.

### 6.2. Metamorphic Minerals

Even though the magmatic evolution comes along with strong compositional heterogeneities at the grain scale, hereafter we focus on the compositional trends observed in metamorphic minerals. Furthermore, a more detailed microstructural classification is proposed in Figure 5 to show the reader the local effects of the inherited compositional heterogeneities.

AmpM$_1$ (Figure 5) is actinolite with Si = 7.78–7.93 apfu, $Al^{VI}$ = 0.02–0.09 apfu, and very low to negligible Ti and Na content (Ti = 0.00–0.02 apfu, $^B$Na = 0.01–0.05 apfu, $^A$Na = 0.00–0.04 apfu). $X_{Mg}$ in AmpM$_1$ is higher in sample Ge11 (0.71–0.77) than in sample Ge8 (0.65–0.53), with the lowest $X_{Mg}$ values where AmpM$_1$ replaces Fe-rich AmpI$_2$. ChlM$_1$ is characterized by $Al^{IV}$ = 0.92–1.09 apfu and $X_{Mg}$ = 0.46–0.56; EpM$_1$ by $Fe^{3+}$ = 0.85–0.93 apfu and $Al^{VI}$ = 2.07–2.14 apfu.

AmpM$_2$ (Figure 5) is actinolite or magnesio-ferri-hornblende, with Si = 7.42–7.83 apfu, $Al^{VI}$ = 0.04–0.17 apfu, and Ti < 0.04 apfu. The Na content in AmpM$_2$ ($^B$Na = 0.02–0.10 apfu, $^A$Na = 0.02–0.13 apfu) is higher than in AmpM$_1$. Even in this case, AmpM$_2$ $X_{Mg}$ in sample Ge11 (0.59–0.81) is generally higher than in sample Ge8 (0.53–0.64), with AmpM$_2$ replacing AmpI$_2$ characterized by the Fe-richest compositions. BtM$_2$ ($X_{Mg}$ = 0.49–0.54) is characterized by Si = 5.38–5.70 apfu, $Al^{VI}$ = 0.46–0.61 apfu, and Ti = 0.06–0.16 apfu (Figure 5). In ChlM$_2$ ($X_{Mg}$ = 0.49–0.55 in sample Ge8, and 0.56–0.59 in sample Ge11) Si is 2.63–2.91 apfu and $Al^{IV}$ is 1.10–1.37 apfu. EpM$_2$ is characterized by $Fe^{3+}$ = 0.75–0.85 apfu and $Al^{VI}$ = 2.15–2.24 apfu (Figure 5). PlM$_2$ is An$_{2-7}$.

Consistent compositional trends characterize the transition from late- to post-intrusive hydrothermalism (M$_1$) to Alpine metamorphism (M$_2$) associated with S3 development:

1. decrease in Fe$^{3+}$ and increase in Al$^{VI}$ from EpM$_1$ to EpM$_2$,
2. increase in Al$^{IV}$ from ChlM$_1$ to ChlM$_2$,
3. decrease in Si and increase in Al$^{VI}$, $^A$Na, and $^B$Na content from AmpM$_1$ to AmpM$_2$.

These trends are diagnostic of a prograde metamorphic evolution through the greenschist facies in mafic rocks (e.g., [60,61] and refs. therein).
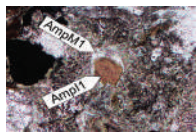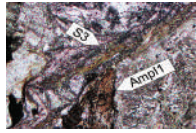
## 7. Metamorphic Evolution

Mineral associations and compositional trends suggest that the metamorphic evolution of the Edolo diabase dykes entirely took place under greenschist facies conditions. It is well known that, under these conditions, equilibrium is often attained only at a very local scale in mafic rocks due to slow reaction progress in the absence of fluids and P-T estimates come along with a wide margin of error [62]. In addition, we have already shown that local compositional heterogeneities inherited from the magmatic evolution persist in these rocks (Figures 4 and 5), making it unwise to use bulk rock data to represent local equilibrium volumes. Taking into account these reasons, we try to constrain the P-T evolution of the Edolo diabase by matching different thermo-barometric methods involving chlorite and amphibole. For chlorite the thermometers that are most suitable in low- to very low-grade rocks [63,64] and avoid the issue of Fe oxidation-state determination (see [64] for a discussion) have been used, even though T > 350 °C should be considered with caution. The same approach was applied in selecting the amphibole thermometers, recalculating the minerals following the procedures suggested by respective authors [65–67] and using only those thermobarometers where greenschist facies conditions are considered.

Chlorite and amphibole thermometry constrain late- to post-intrusive hydrothermal conditions (M$_1$). According to ChlM$_1$ thermometry (Table 1; [63,64]), temperatures are slightly lower than 300 °C, while AmpM$_1$ thermometry suggest temperatures at around 350 °C (Table 1; [65]).

The physical conditions of Alpine metamorphism (M$_2$) are constrained by chlorite and amphibole thermobarometry. ChlM$_2$ thermometry [63,64] returns temperatures between 300 and 420 °C (Table 1). However, these authors reccomend caution when dealing with results above 350 °C. Temperatures above 350 °C are indicated by AmpM$_2$ thermometry ([65], Figure 6), whereas pressures up to 0.2 GPa are indicated by AmpM$_2$ barometry ([66,67], Figure 6).

A further constrain on the P-T evolution of the Edolo diabase dykes comes from the country rocks, where S3 is marked by chlorite and white mica. We thus consider the biotite appearance at a temperature of 420 °C [62] as the upper temperature boundary for the Alpine metamorphic evolution of the Edolo diabase. Therefore we suggest that Alpine P-T conditions are constrained between T = 350–420 °C and P ≤ 0.2 GPa (Figure 6).

**Table 1.** Thermobarometric constraints on M$_1$ and M$_2$ minerals.

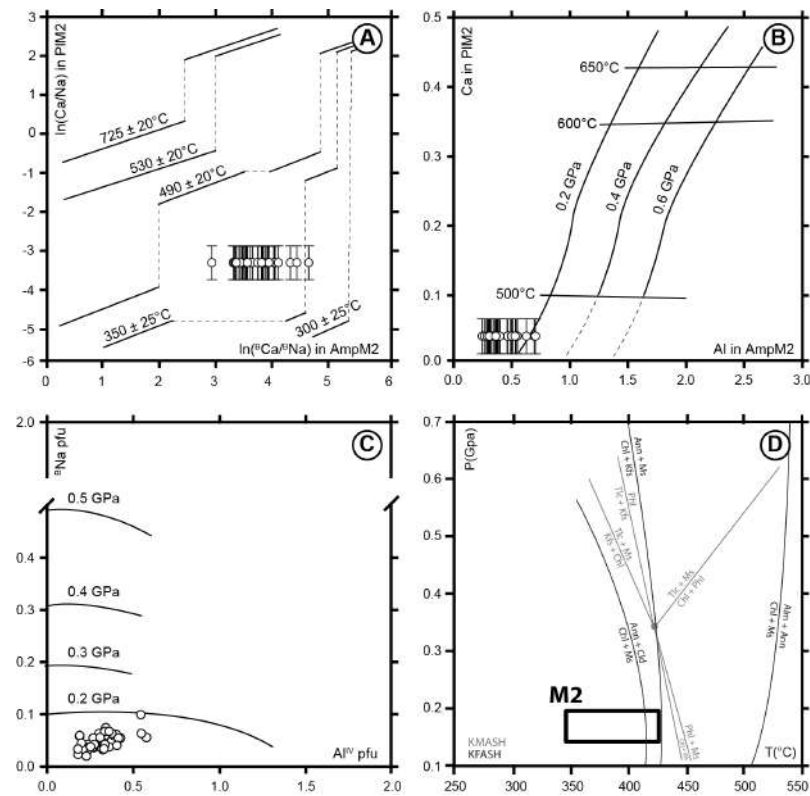| Metamorphic Stage | Microstructure | T$_{Chl}$ [63,64] | T$_{Amp-Pl}$ [65,67] | P$_{Amp}$ [66,67] |
|---|---|---|---|---|
| M$_1$ |  | 230–290 °C (n = 3) | 290 °C < T ≪ 490 °C (n = 12) | ≪0.2 GPa (n = 12) |
| M$_2$ |  | 300–420 °C (n = 16) | 350 °C ≤ T < 490 °C (n = 41) | ≤0.2 GPa (n = 41) |

**Figure 6.** Thermobarometric constrains on $M_2$ minerals. (**A**): amphibole−plagioclase thermometer of [65]; (**B**): amphibole−plagioclase thermo−barometer of [67]; (**C**) amphibole barometer of [66]; (**D**): P-T conditions accountable for $M_2$ minerals development (black box). KFASH and KMASH reactions are taken from [62,68].

## 8. Discussion

North of the Orobic–Porcile–Gallinera thrust system, the alkaline Edolo diabase dykes are crosscut by Alpine S3 foliation. In the dykes, S3 is marked by Al- and Na-rich actinolite (Amp$M_2$), biotite (Bt$M_2$), chlorite (Chl$M_2$), epidote (Ep$M_2$), albite (Pl$M_2$), and titanite. In the host metapelites, S3 is instead marked by white mica, chlorite, and opaque minerals. S3 development is kinematically correlated with the development of the Orobic–Porcile–Gallinera thrust system (D3) and chevron-type D3 folding in the Variscan basement rocks [16,20,21,47,48].

Taking into account textural and compositional heterogeneities in the samples, their influence on the determination of equilibrium P-T conditions, and the intrinsic error of the thermo-barometric methods at low grade metamorphic conditions, we suggest that S3 developed in the Edolo diabase at T = 350–420 °C and P ≤ 0.2 GPa, as indicated by overlapping thermo-barometric estimates. These P-T conditions are the first quantitative estimates of Alpine metamorphic conditions in the Southern Alps that were attained during a prograde evolution following a former re-equilibration stage ($M_1$) at T ≤ 350 °C related to post-intrusive hydrothermal circulation.

Metamorphic assemblages that suggest P-T conditions similar to those estimated for the Edolo diabase dykes are also described in the pre-Alpine mafic dykes at the junction between the Orobic and Porcile thrusts ([20], Figure 1), indicating that also the western edge of the Orobic–Porcile thrust nappe recorded the same metamorphic imprint during the Alpine convergence. The onset of south-verging shortening (syn-D3) in the Southern Alps occurred during oceanic subduction, as indicated by the 80–43 Ma $^{40}$Ar/$^{39}$Ar ages of the Orobic–Porcile thrusts [10,11] in comparison with the ages of HP rocks in the exhumed Alpine subduction zone ([1–3] and refs. therein). This time interval is therefore considered for the upper greenschist facies Alpine metamorphism ($M_2$) recorded in the Edolo diabase dykes.

The obtained P-T conditions suggest a minimal T/depth ratio of 50–60 °C that is compatible with volcanic arc geothermal gradients (e.g., [69–71], Figure 7). Such perturbed thermal state in the upper-plate of the Alpine subduction system can also explain the genesis of the syn-subductive magmatism south of the Periadriatic fault system, in the Veneto volcanic province (~40 Ma, [72] and ref. therein) and in the southern Adamello pluton (43–41 Ma, [73,74]).
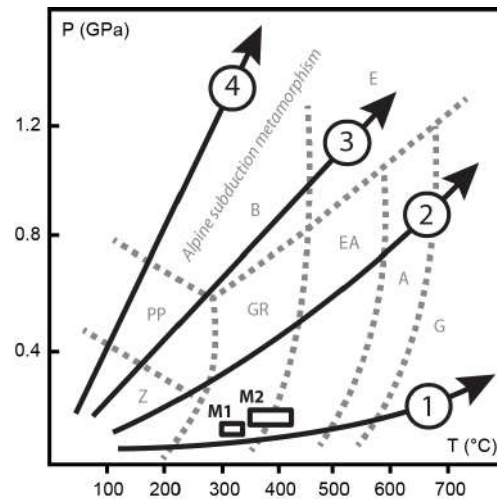


**Figure 7.** Metamorphic conditions attained by the Edolo diabase dykes during post-emplacement ($M_1$) and Alpine syn-D3 ($M_2$) evolution. Metamorphic facies after [75]–Z: zeolite; PP: prehnite-pumpellyite; B: blueschist; GR: greenschist; EA: epidote amphibolite; A: amphibolite; E: eclogite; G: granulite. P-T trajectories are–1: active arc volcanoes; 2: normal geothermal gradients at plate interior; 3: "warm" subduction zones; 4: "cold" subduction zones ([69] and refs. therein). "Alpine subduction metamorphism" locates metamorphic conditions recorded by rocks involved in the Alpine subduciton system.

## 9. Conclusions

In this contribution we investigated the thermal state attained by the upper plate of the Alpine subduction system, i.e., the central Southalpine domain, looking at the structural and metamorphic evolution retained by the Edolo diabase dykes north of the Orobic–Porcile–Gallinera thrust system and south of the Periadriatic fault system. The dykes retain two metamorphic events, the first ($M_1$) at T < 350 °C interpreted as due to a post-intrusive hydrothermal activity and the second ($M_2$) at T = 350–420 °C, P ≤ 0.2 GPa, which is syn-kynematic with the development of D3 south-verging Alpine thust system between 80 and 43 Ma. $M_2$ metamorphism developed under a thermal state compatible with a syn-subductive volcanic arc. South of the Periadriatic fault system, which borders the exhumed Alpine subduction zone, magmatic bodies emplaced intersecting D3 structures during active Alpine subduction in Eocene times.

**Author Contributions:** Conceptualization, M.F., D.Z., G.R., M.R., A.R., J.-M.L. and M.I.S.; Investigation, M.F., D.Z., G.R., M.R., A.R., J.-M.L. and M.I.S.; Methodology, M.F., D.Z., G.R., M.R., A.R., J.-M.L. and M.I.S.; Supervision, D.Z., G.R., J.-M.L. and M.I.S.; Writing—original draft, M.F., D.Z., G.R., M.R., A.R., J.-M.L. and M.I.S.; Writing—review & editing, M.F., D.Z., G.R., M.R., A.R., J.-M.L. and M.I.S. All authors have read and agreed to the published version of the manuscript.

## References

1. Schmid, S.M.; Fügenschuh, B.; Kissling, E.; Schuster, R. Tectonic map and overall architecture of the Alpine orogen. *Eclogae Geol. Helv.* **2004**, *97*, 93–117. [CrossRef]
2. Dal Piaz, G.V. The Italian Alps: A journey across two centuries of Alpine geology. *J. Virtual Explor.* **2010**, *36*, 77–106. [CrossRef]
3. Lardeaux, J.-M. Deciphering orogeny: A metamorphic perspective. Examples from European Alpine and Variscan belts: Part I: Alpine metamorphism in the western Alps. A review. *Bulletin de la Société Géologique de France* **2014**, *185*, 93–114. [CrossRef]
4. Ford, M.; Lickorish, W.H. Foreland basin evolution around the western Alpine Arc. *Geol. Soc. Lond. Spec. Publ.* **2004**, *221*, 39–63. [CrossRef]
5. Roll, Y.; Cox, S.; Boullier, A.M.; Pennacchioni, G.; Mancktelow, N. Rare earth and trace element mobility in mid-crustal shear zones: Insights from the Mont Blanc Massif (Western Alps). *Earth Planet. Sci. Lett.* **2003**, *214*, 203–219.
6. Sanchez, G.; Rolland, Y.; Schneider, J.; Corsini, M.; Oliot, E.; Goncalves, P.; Verati, C.; Lardeaux, J.-M.; Marquer, D. Dating low-temperature deformation by 40Ar/39Ar on white mica, insights from the Argentera-Mercantour Massif (SW Alps). *Lithos* **2011**, *125*, 521–536. [CrossRef]
7. Cenki-Tok, B.; Darling, J.R.; Rolland, Y.; Dhuime, B.; Storey, C.D. Direct dating of mid-crustal shear zones with synkinematic allanite: New in situ U-Th-Pb geochronological approaches applied to the Mont Blanc massif. *Terra Nova* **2014**, *26*, 29–37. [CrossRef]
8. Filippi, M.; Zanoni, D.; Gosso, G.; Lardeaux, J.-M.; Verati, C.; Spalla, M.I. Structure of lamprophyres: A discriminant marker for Variscan and Alpine tectonics in the Argentera-Mercantour Massif, Maritime Alps. *BSGF-Earth Sci. Bull.* **2019**, *190*, 12. [CrossRef]
9. Filippi, M.; Zanoni, D.; Lardeaux, J.-M.; Spalla, M.I.; Gosso, G. Evidence of Tethyan continental break-up and Alpine collision in the Argentera-Mercantour Massif, Western Alps. *Lithos* **2020**, *372–373*, 105653. [CrossRef]
10. Zanchetta, S.; D'Adda, P.; Zanchi, A.; Barberini, V.; Villa, I.M. Cretaceous-Eocene compression in the central Southern Alps (N Italy) inferred from 40Ar/39Ar dating of pseudotachylytes along regional thrust faults. *J. Geodyn.* **2011**, *51*, 245–263. [CrossRef]
11. Zanchetta, S.; Malusà, M.G.; Zanchi, A. Precollisional development and Cenozoic evolution of the Southalpine retrobelt (European Alps). *Lithosphere* **2015**, *7*, 662–681. [CrossRef]
12. Crespi, R.; Liborio, G.; Mottana, A. On a widespread occurrence of stilpnomelane to the South of the Insubric line, Central Alps, Italy. *Neues Jahrb. Für Mineral. Monatshefte* **1982**, *6*, 265–271.
13. Brack, P. Structures in the Southwestern border of the Adamello intrusion (Alpi Bresciane, Italy). *Schweiz. Mineral. Petrogr. Mitteilungen* **1981**, *61*, 37–50.
14. Brack, P. Geologie der Itrusiva und Rahmengesteine des Südwest-Adamello (Nord-Italien). Ph.D. Thesis, ETH, Zurich, Switzerland, 1984.
15. Cassinis, G.; Dal Piaz, G.V.; Eusebio, A.; Gosso, G.; Martinotti, G.; Massari, F.; Milano, P.F.; Pennacchioni, G.; Perello, M.; Pessina, C.M.; et al. Report on a structural and sedimentological analysis in the Uranium Province of the Orobic Alps. *Uranium* **1986**, *2*, 241–260.
16. Milano, P.F.; Pennacchioni, G.; Spalla, M.I. Alpine and pre-Alpine tectonics in the Central Orobic Alps (Southern Alps). *Eclogae Geol. Helv.* **1988**, *81*, 273–293.
17. Albini, S.; Battaglia, D.; Bellini, G.; Bigoni, C.; Carminati, E.; Ceriani, S.; Forcella, F.; Gosso, G.; Guizzetti, A.; Oliva, G.; et al. Alpine deformations and pre-Alpine remnants in the north-eastern Orobic Alps, Southalpine Belt. *Quad. Geodin. Alp. Quat.* **1994**, *2*, 25–39.
18. Cadel, G.; Cosi, M.; Pennacchioni, G.; Spalla, M.I. A new map of the Permo-Carboniferous cover and Variscan metamorphic basement in the Central Orobic Alps, Southern Alps-Italy. *Mem. Sci. Geol. Padova* **1996**, *48*, 1–53.
19. Gosso, G.; Spalla, M.I.; Bini, A.; Siletto, G.B.; Berra, F.; Forcella, F. *Note Illustrative Della Carta Geologica d 'Italia alla Scala 1: 50.000, Foglio 057 Malonno*; ISPRA and Regione Lombardia: Malonno, Italy, 2012.
20. D'Adda, P.; Zanchetta, S. Geological-structural map of the Orobic and Porcile thrust junction, central southern Alps (N Italy). *J. Maps* **2015**, *11*, 25–38. [CrossRef]
21. Rebay, G.; Maroni, M.; Siletto, G.B.; Spalla, M.I. Superposed syn-metamorphic structures of the Alpine and pre-Alpine convergent cycles in the Southalpine basement of the Orobic Alps (Northern Italy). *J. Maps* **2015**, *11*, 168–180. [CrossRef]
22. Schiavinato, G. Sulle rocce diabasiche comprese negli Scisti di Edolo in Val Camonica (Lombardia). *Rend. Della Soc. Mineral. Ital.* **1954**, *11*, 233–261.
23. Polino, R.; Dal Piaz, G.V.; Gosso, G. Tectonic erosion at the Adria margin and accretionary processes for the Cretaceous orogeny of the Alps. *Mémoires de la Société Géologique de France* **1990**, *156*, 345–367.
24. Zanoni, D.; Spalla, M.I. The Variscan evolution in basement cobbles of the Permian Ponteranica Formation by microstructural and petrologic analysis. *Ital. J. Geosci.* **2018**, *137*, 254–271. [CrossRef]

25. Filippi, M.; Spalla, M.I.; Pigazzini, N.; Diella, V.; Lardeaux, J.-M.; Zanoni, D. Cld-St-And-bearing assemblages in the central Southalpine Basement: Markers of an evolving thermal regime during Variscan convergence. *Minerals* **2021**, *11*, 1124. [CrossRef]

26. Schmid, S.M.; Aebli, H.R.; Heller, F.; Zingg, A. The role of the Periadriatic Line in the tectonic evolution of the Alps. *Geol. Soc. Lond. Spec. Publ.* **1989**, *45*, 153–171. [CrossRef]

27. Müller, W.; Prosser, G.; Mancktelow, N.S.; Villa, I.M.; Kelley, S.P.; Viola, G.; Oberli, F. Geochronological constraints on the evolution of the Periadriatic Fault System (Alps). *Int. J. Earth Sci.* **2001**, *90*, 623–653. [CrossRef]

28. Oberli, F.; Meier, M.; Berger, A.; Rosenberg, C.L.; Gieré, R. U-Th-Pb and 230Th/238U disequilibrium isotope systematics: Precise accessory mineral chronology and melt evolution tracing in the Alpine Bergell intrusion. *Geochim. Cosmochim. Acta* **2004**, *68*, 2543–2560. [CrossRef]

29. Rosenberg, C.L. Shear zones and magma ascent: A model based on a review of the Tertiary magmatism in the Alps. *Tectonics* **2004**, *23*. [CrossRef]

30. Gazzola, D.; Gosso, G.; Pulcrano, E.; Spalla, M.I. Eo-Alpine HP metamorphism in the Permian intrusives from the steep belt of the central Alps (Languard-Campo nappe and Tonale Series). *Geodin. Acta* **2000**, *13*, 149–167. [CrossRef]

31. Salvi, F.; Spalla, M.I.; Zucali, M.; Gosso, G. Three-dimensional evaluation of fabric evolution and metamorphic reaction progress in polycyclic and polymetamorphic terrains: A case from the Central Italian Alps. *Geol. Soc. Lond. Spec. Publ.* **2010**, *332*, 173–187. [CrossRef]

32. Roda, M.; Zucali, M.; Li, Z.X.; Spalla, M.I.; Yao, W. Pre-alpine contrasting tectono-metamorphic evolutions within the Southern Steep Belt, Central Alps. *Lithos* **2018**, *310*, 31–49. [CrossRef]

33. Picazo, S.M.; Ewing, T.A.; Müntener, O. Paleocene metamorphism along the Pennine–Austroalpine suture constrained by U–Pb dating of titanite and rutile (Malenco, Alps). *Swiss J. Geosci.* **2019**, *112*, 517–542. [CrossRef]

34. Diella, V.; Spalla, M.I.; Tunesi, A. Contrasting thermomechanical evolutions in the Southalpine metamorphic basement of the Orobic Alps (Central Alps, Italy). *J. Metamorph. Geol.* **1992**, *10*, 203–219. [CrossRef]

35. Bertotti, G.; Siletto, G.B.; Spalla, M.I. Deformation and metamorphism associated with crustal rifting: The Permian to Liassic evolution of the Lake Lugano-Lake Como area (Southern Alps). *Tectonophysics* **1993**, *226*, 271–284. [CrossRef]

36. Spalla, M.I.; Zanoni, D.; Marotta, A.M.; Rebay, G.; Roda, M.; Zucali, M.; Gosso, G. The transition from Variscan collision to continental break-up in the Alps: Insights from the comparison between natural data and numerical model predictions. *Geol. Soc. Lond. Spec. Publ.* **2014**, *405*, 363–400. [CrossRef]

37. Spalla, M.I.; Gosso, G. Pre-Alpine tectonometamorphic units in the central Southern Alps: Structural and metamorphic memory. *Mem. Sci. Geol. Padova* **1999**, *51*, 221–229.

38. Garzanti, E.; Schiunnach, D. International ophiolite symposium field excursion guide-continental rifting to ocean floor metamorphism (21st–23rd September 1995): First day-Permo-Triassic evolution-constraints from the sedimentary records. *Ofioliti* **1997**, *22*, 147–152.

39. Spalla, M.I.; Zanoni, D.; Gosso, G.; Zucali, M. Deciphering the geologic memory of a Permian conglomerate of the Southern Alps by pebble P–T estimates. *Int. J. Earth Sci.* **2009**, *98*, 203–226. [CrossRef]

40. Zanoni, D.; Spalla, M.I.; Gosso, G. Vestiges of lost tectonic units in conglomerate pebbles? A test in Permian sequences of the Southalpine Orobic Alps. *Geol. Mag.* **2010**, *147*, 98–122. [CrossRef]

41. Cassinis, G.; Perotti, C.R.; Ronchi, A. Permian continental basins in the Southern Alps (Italy) and peri-mediterranean correlations. *Int. J. Earth Sci.* **2012**, *101*, 129–157. [CrossRef]

42. Berra, F.; Tiepolo, M.; Caironi, V.; Siletto, G.B. U-Pb zircon geochronology of volcanic deposits from the Permian basin of the Orobic Alps (Southern Alps, Lombardy): Chronostratigraphic and geological implications. *Geol. Mag.* **2015**, *152*, 429–443. [CrossRef]

43. Berra, F.; Felletti, F.; Tessarollo, A. Stratigraphic architecture of a transtensional continental basin in low-altitude semiarid conditions: The Permian succession of the central Orobic basin (Southern Alps, Italy). *J. Sediment. Res.* **2016**, *86*, 408–429. [CrossRef]

44. Wennekers, J.H.L. The structure of Bergamo Alps compared with that of the North-West Highlands of Scotland. *Leid. Geol. Meded.* **1932**, *4*, 83–93.

45. De Sitter, L.U. La structure des Alpes Lombardes. *Livre Mémoire Paul Fallot* **1963**, *2*, 245–256.

46. Schönborm, G. Alpine tectonics and kinematic models of the central Southern Alps. *Mem. Sci. Geol. Padova* **1992**, *44*, 229–393.

47. Carminati, E.; Siletto, G.B.; Battaglia, D. Thrust kinematics and internal deformation in basement involved foreland fold and thrust belts: The Eastern Orobic Alps case (Central Southern Alps, Northern Italy). *Tectonics* **1997**, *16*, 259–271. [CrossRef]

48. Ghiselli, A.; Zucali, M.; Bini, A. Structural and geomorphological map of the Passo San Marco–Pizzo di Trona area (Western Orobic Alps, southern Alps, Italy). *J. Maps* **2015**, *11*, 56–65. [CrossRef]

49. Schaltegger, U.; Nowak, A.; Ulianov, A.; Fisher, C.M.; Gerdes, A.; Spikings, R.; Whitehouse, M.J.; Bindeman, I.; Hanchar, J.M.; Duff, J.; et al. Zircon Petrochronology and 40Ar/39Ar Thermochronology of the Adamello Intrusive Suite, N. Italy: Monitoring the Growth and Decay of an Incrementally Assembled Magmatic System. *J. Petrol.* **2019**, *60*, 701–722. [CrossRef]

50. Bersezio, R.; Fornaciari, M.; Gelati, R.; Napolitano, A.; Valdisturlo, A. The significance of the Upper Cretaceous to Miocene clastic wedges in the deformation history of the Lombardian southern Alps. *Géologie Alp.* **1993**, *69*, 3–20.

51. Viganò, A.; Tumiati, S.; Recchia, S.; Martin, S.; Marelli, M.; Rigon, R. Carbonate pseudotachylytes: Evidence for seismic faulting along carbonate faults. *Terra Nova* **2011**, *23*, 187–194. [CrossRef]

52. D'Adda, P.; Zanchi, A.; Bergomi, M.; Berra, F.; Malusà, M.G.; Tunesi, A.; Zanchetta, S. Polyphase thrusting and dyke emplacement in the central Southern Alps (Northern Italy). *Int. J. Earth Sci.* **2011**, *100*, 1095–1113. [CrossRef]

53. Bergomi, M.A.; Zanchetta, S.; Tunesi, A. The Tertiary dike magmatism in the Southern Alps: Geochronological data and geodynamic significance. *Int. J. Earth Sci.* **2015**, *104*, 449–473. [CrossRef]

54. Le Maitre, R.W.; Streckeisen, A.; Zanettin, B.; Le Bas, M.J.; Bonin, B.; Bateman, P. *Igneous Rocks: A Classification and Glossary of Terms: Recommendations of the International Union of Geological Sciences Subcommission on the Systematics of Igneous Rocks*; Cambridge University Press: Cambridge, UK, 2002; p. 236.

55. Casetta, F.; Ickert, R.B.; Mark, D.F.; Bonadiman, C.; Giacomoni, P.P.; Ntaflos, T.; Coltorti, M. The alkaline lamprophyres of the Dolomitic Area (Southern Alps, Italy): Markers of the Late Triassic change from orogenic-like to anorogenic magmatism. *J. Petrol.* **2019**, *60*, 1263–1298. [CrossRef]

56. Blom, J.C.; Passchier, C.W. Structures along the Orobic thrust, Central Orobic Alps, Italy. *Geol. Rundsch.* **1997**, *86*, 627–636. [CrossRef]

57. Spalla, M.I.; Carminati, E.; Ceriani, S.; Oliva, A.; Battaglia, D. Influence of deformation partitioning and metamorphicre-equilibration on P–T path reconstruction in the pre-Alpine basement of central Southern Alps (Northern Italy). *J. Metamorph. Geol.* **1999**, *17*, 319–336. [CrossRef]

58. Locock, A.J. An Excel spreadsheet to classify chemical analyses of amphiboles following the IMA 2012 recommendations. *Comput. Geosci.* **2014**, *62*, 1–11. [CrossRef]

59. Ridolfi, F.; Renzulli, A. Calcic amphiboles in calc-alkaline and alkaline magmas: Thermobarometric and chemometric empirical equations valid up to 1130 °C and 2.2 GPa. *Contrib. Mineral. Petrol.* **2012**, *163*, 877–895. [CrossRef]

60. Maruyama, S.; Suzuki, K.; Liou, J.G. Greenschist–amphibolite transition equilibria at low pressures. *J. Petrol.* **1983**, *24*, 583–604. [CrossRef]

61. Thompson, A.B.; Laird, J. Calibrations of modal space for metamorphism of mafic schist. *Am. Mineral.* **2005**, *90*, 843–856. [CrossRef]

62. Bucher, K.; Frey, M. *Petrogenesis of Metamorphic Rocks*; Springer: Berlin/Heidelberg, Germany, 2002; p. 341.

63. Cathelineau, M. Cation site occupancy in chlorites and illites as a function of temperature. *Clay Miner.* **2019**, *23*, 471–485. [CrossRef]

64. Bourdelle, F.; Parra, T.; Chopin, C.; Beyssac, O. A new chlorite geothermometer for diagenetic to low-grade metamorphic conditions. *Contrib. Mineral. Petrol.* **2013**, *165*, 723–735. [CrossRef]

65. Spear, F.S. NaSi- CaAl exchange equilibrium between plagioclase and amphibole. *Contrib. Mineral. Petrol.* **1980**, *72*, 33–41. [CrossRef]

66. Brown, E.H. The crossite content of Ca-amphibole as a guide to pressure of metamorphism. *J. Petrol.* **1977**, *18*, 53–72. [CrossRef]

67. Plyusnina, L.P. Geothermometry and geobarometry of plagioclase-hornblende bearing assemblages. *Contrib. Mineral. Petrol.* **1982**, *80*, 140–146. [CrossRef]

68. Spear, F.S. *Metamorphic Phase Equilibria and Pressure-Temperature-Time Paths*; Mineralogical Society of America Monograph: Washington, DC, USA, 1995; p. 799.

69. Cloos, M. Lithospheric buoyancy and collisional orogenesis: Subduction of oceanic plateaus, continental margins, island arcs, spreading ridges, and seamounts. *Geol. Soc. Am. Bull.* **1993**, *105*, 715–737. [CrossRef]

70. Rothstein, D.A.; Manning, C.E. Geothermal gradients in continental magmatic arcs; constraints from the eastern Peninsular Ranges Batholith, Baja California, Mexico. In *Tectonic Evolution of North West-Ern Mexico and the Southwestern USA*; Johnson, S., Paterson, S., Fletcher, J., Girty, G., Kimbrough, D., Martin-Barajas, A., Eds.; Geological Society of America: Boulder, CO, USA, 2003; pp. 337–354.

71. Verati, C.; Lardeaux, J.M.; Favier, A.; Corsini, M.; Philippon, M.; Legendre, L. Arc-related metamorphism in the Guadeloupe archipelago (Lesser Antilles active island arc): First report and consequences. *Lithos* **2018**, *320*, 592–598. [CrossRef]

72. Bartoli, O.; Meli, S.; Sassi, R.; Magaraci, D. Amphiboles and clinopyroxenes from Euganean (NE Italy) cumulus enclaves: Evidence of subduction-related melts below Adria microplate. *Rend. Lincei* **2013**, *24*, 151–161. [CrossRef]

73. Tiepolo, M.; Tribuzio, R.; Langone, A. High-Mg andesite petrogenesis by amphibole crystallization and ultramafic crust assimilation: Evidence from Adamello hornblendites (Central Alps, Italy). *J. Petrol.* **2011**, *52*, 1011–1045. [CrossRef]

74. Ji, W.Q.; Malusà, M.G.; Tiepolo, M.; Langone, A.; Zhao, L.; Wu, F.Y. Synchronous Periadriatic magmatism in the Western and Central Alps in the absence of slab breakoff. *Terra Nova* **2019**, *31*, 120–128. [CrossRef]

75. Ernst, W.G. *Petrologic Phase Equilibria*; Freeman and Company: San Francisco, CA, USA, 1976; p. 333.